Atomic-scale friction observed with a two-dimensional frictional-force microscope

Satoru Fujisawa, Eigo Kishi, Yasuhiro Sugawara, and Seizo Morita
Department of Physics, Faculty of Science, Hiroshima University, Higashi-Hiroshima 724, Japan
(Received 8 July 1994; revised manuscript received 15 November 1994)

Using the two-dimensional frictional-force microscope, we studied the two-dimensional nature of the atomic-scale friction between a Si_3N_4 tip and the cleaved MoS_2 surface. As a result, we confirmed the existence of two-dimensionally discrete friction with the lattice periodicity of the MoS_2 surface. In addition to the well-known stick-slip behavior, we found the appearance of friction with square-wave behavior which works across the scanning direction, although it is contradictory to the assumption of classical friction. We found that this friction is due to spatially discrete adhesion and jumps with the lattice periodicity, which is explained by the two-dimensional stick-slip model not only qualitatively but also quantitatively. We also observed the fluctuation of the discrete jumps. Further, using the two-dimensional stick-slip model with an effective adhesive radius, we explain the sawtooth and square-wave behaviors due to each discrete jump in more detail.

I. INTRODUCTION

Friction is a familiar phenomenon which always occurs between two sliding surfaces. At the macroscopic interface, numerous asperities are in contact, where the adhesion between the asperities contributes to the frictional force.[1] Thus, to understand the friction further, it is necessary to study the simple system, for instance the friction between a single apserity and an atomically flat surface. Frictional-force microscopy (FFM) (Ref. 2) enables us to investigate a single asperity friction on an atomic scale. FFM investigations explored atomic-scale friction,[2–4] and microtribology,[5] i.e., friction, lubrication, and wear on microscale to nanoscale.[6,7] On the other hand, in FFM investigations so far only one component of the frictional force vector was studied, although the frictional force vector at the interface is a two- or three-dimensional vector. Thus only a part of the properties of the friction seems to have been studied.

In the present paper, we study the two-dimensional nature of the atomic-scale friction between a single apserity of an atomic force microscope (AFM) tip and a cleaved MoS_2 surface using a two-dimensional frictional-force microscope (2D-FFM),[8,9] based on the two-dimensional stick-slip model.[8] We extend the two-dimensional stick-slip model by introducing an effective adhesive radius, which provides further understanding of the two-dimensional nature.

II. TWO-DIMENSIONAL FRICTIONAL-FORCE MICROSCOPE (2D-FFM)

A. Force components measured by AFM/LFM

First we discuss force components[10,11] of the normal reacting force and the frictional force measured with an atomic force/lateral force microscope (AFM/LFM) using the optical lever deflection method with a quadrant position-sensitive detector.[12,13] The AFM/LFM detects angle changes of the torsion and deflection of the cantilever, separately and simultaneously. On the other hand, in general, force is a three-dimensional vector. So the force which acts on the tip apex of a cantilever has X, Y, and Z components, which we call F_X, F_Y, and F_Z, respectively. The angle change of the deflection is caused by both F_Y and F_Z, while the angle change of the torsion is caused only by F_X. Here, as shown in Fig. 1, we define the X, Y, and Z directions as across, along, and perpendicular to the cantilever, respectively.

In the contact mode, both frictional and normal reacting forces act on the tip apex of the cantilever. Both forces should have X, Y, and Z components, which we call (f_X, f_Y, and f_Z) and (N_X, N_Y, and N_Z), respectively. Thus we have

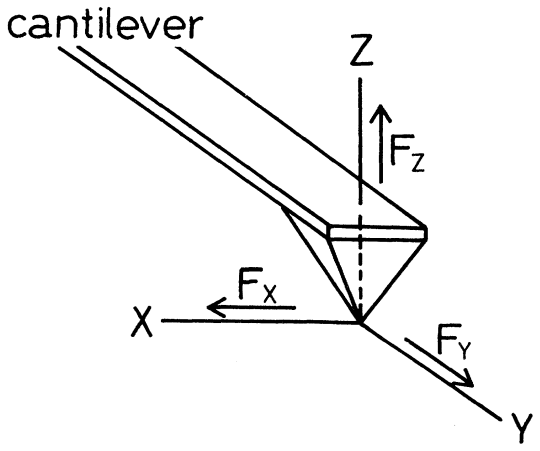

FIG. 1. Schematic representation of the X, Y, and Z directions. The X, Y, and Z directions are defined as the directions across, along, and normal to the cantilever, respectively.

$$F_X = f_X + N_X ,$$
$$F_Y = f_Y + N_Y , \quad (1)$$
$$F_Z = f_Z + N_Z .$$

B. Interpretation of AFM/LFM as a 2D-FFM

On an atomically flat surface, we obtain

$$N_X = N_Y = f_Z = 0 \ \text{(zero)} , \quad (2)$$

so we have

$$F_X = f_X ,$$
$$F_Y = f_Y , \quad (3)$$
$$F_Z = N_Z .$$

As a result, the angle change of the deflection is caused both by f_Y and N_Z, while the angle change of the torsion is caused only by f_X. Then the deflection output of V_{def} due to the angle change of the deflection is given by

$$V_{\text{def}} = AF_Z/k_Z + BF_Y/k_Y = AN_Z/k_Z + Bf_Y/k_Y . \quad (4)$$

The torsion output of V_{tor} due to the angle change of the torsion is given by

$$V_{\text{tor}} = CF_X/k_X = Cf_X/k_X . \quad (5)$$

Here k_X, k_Y, and k_Z and A, B, and C are the spring constant and output sensitivity of X, Y, and Z, respectively. When f_Y is much larger than N_Z, as is often the case with the layered materials,[8,9,14–16] the deflection is dominated by f_Y, i.e.,

$$V_{\text{def}} \doteq Bf_Y/k_Y . \quad (6)$$

So the deflection and torsion are caused by f_Y and f_X, respectively, when

$$f_Y \gg N_Z . \quad (7)$$

Thus the AFM/LFM could be interpreted as a 2D-FFM.

III. EXPERIMENT

In the present experiment, with the 2D-FFM described above, we measured the two-dimensional frictional-force vector (f_X, f_Y) between the tip apex and the atomically flat surface with a raster scan through $V_{\text{def}}(=Bf_Y/k_Y)$ and $V_{\text{tor}}(=Cf_x/k_X)$ under the variable deflection mode. As a result, we obtained both f_X and f_Y, which are measured simultaneously. Here we used a weak feedback control of the Z direction to the deflection signal in order to compensate for the Z direction drift. As an atomically flat surface, we used a cleaved (0001) surface of MoS_2. Its lattice structure shows threefold symmetry with a lattice constant of 3.16 Å.[17] Soon after the cleavage of the surface, measurements were performed in air under ambient condition. As a cantilever, we used a rectangular microcantilever[18] with ~250-Å radius of curvature on a sharp tip apex, which is made of Si_3N_4. Its length, width, and thickness are 100, 40, and 0.8 μm, respectively. Its calculated spring constants of the deflection and torsion are $k_Z = 0.75$ and $k_X = 550$ N/m, respectively. We set the repulsive force at $\sim 1.8 \times 10^{-7}$ N. The raster scan rate was set at ~400 Å/s for the fast-line scan and ~0.80 Å/s for the slow scan.

IV. RESULTS AND DISCUSSION

A. Frictional-force images with the lattice periodicity

Figures 2(a) and 2(b) show f_X (left) and f_Y (right) images obtained for the fast-line-scan directions along and across the cantilever, i.e., the Y and X directions, respectively. These images were obtained by stacking the fast-line-scan data step by step toward the slow-scan direction. Here the magnitudes of f_X and f_Y were indicated by the brightness, and the fast-line scan and slow scan were performed from the left to right and from the bottom to top of the images, respectively. Thus the changes of the fast-line-scan data due to the slow scan create the contrast of these images. If we ignore the fine structures or small differences, they all seem to have threefold symmetry with a periodicity of 3.1±0.3 Å, which agrees well with the lattice constant of the cleaved MoS_2 surface. This implies that the change of the two-dimensional frictional-force vector has the lattice periodicity.

B. Two-dimensionally discrete friction with the lattice periodicity

To investigate the nature of the two-dimensional frictional-force vector imaged by the raster scan, i.e., the mechanism of the atomic-scale friction with the lattice periodicity, we analyzed all fast-line-scan data.

1. Atomic-scale friction across the scan direction

Figure 3(a) shows typical data due to a single fast-line scan obtained at the place indicated by the thick arrow in Fig. 2(a). Upper and lower data correspond to f_X and f_Y, respectively. f_X shows the square-wave behavior comprised of a sharp steplike rise and fall with a constant amplitude, while f_Y shows the sawtooth behavior in which the sharp rise is synchronized with the steplike rise and fall in the square-wave behavior. The periodicity of the square-wave behavior is 5.4±0.6 Å, while the periodicity of the sawtooth behavior is 2.7±0.3 Å, i.e., half the square-wave behavior. The sawtooth behavior in the f_Y is due to well-known stick-slip motion of the tip apex[2,3,8,9,14–16] induced by friction.

Further, the f_X with square-wave behavior indicates the appearance of the friction which works across the fast-line-scan direction. That is, the two-dimensional frictional-force vector with nonzero f_X and f_Y components is not parallel to the scanning direction, although

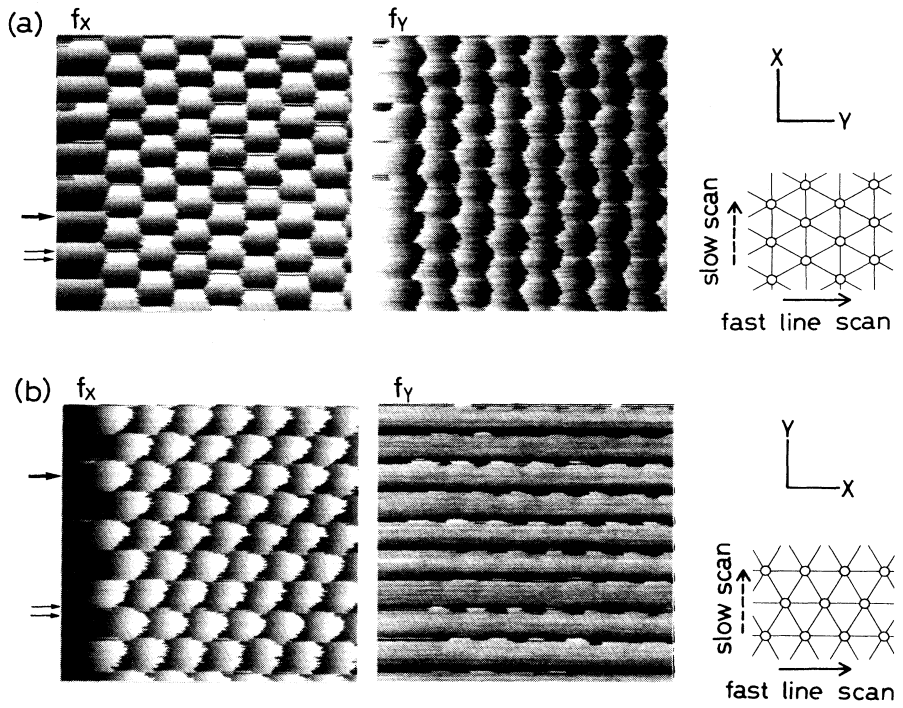

FIG. 2. f_X and f_Y images for the fast-line-scan directions (a) along the cantilever (along the Y direction) and (b) across the cantilever (along the X direction). Scan area is 25×25 Å^2. Beside each image, schematic views of the lattice structure of the observed MoS_2 surface are shown.

this is contradictory to the assumption of macroscopic (classical) friction.

Figure 3(b) shows typical data due to a single fast-line scan obtained at the place indicated by the thick arrow in Fig. 2(b). f_X shows the well-known sawtooth behavior with a periodicity of 3.1 ± 0.3 Å, while f_Y shows no fine structure within the noise level.

2. *Spatially discrete adhesion and jumps*

From the periodic sawtooth behaviors of f_Y in Fig. 3(a) and f_X in Fig. 3(b), we conjectured the presence of spatially discrete adhesion points, namely stick points.[8] Further, from the frictional-force component images with lattice periodicity in Figs. 2(a) and 2(b), we proposed a two dimensional stick-slip model,[8] where the stick points distribute two dimensionally with a lattice periodicity of the MoS_2 surface, as shown in Fig. 3(c). As result, the tip apex slips or jumps two dimensionally from one stick point to the nearest stick point for the fast-line-scan direction.

Based on the two-dimensional stick-slip model, for the fast-line scan toward the Y direction, the tip apex will take a zigzag walk with the stick-slip motion as shown in Fig. 3(c). Thus f_Y will show the well-know sawtooth behavior with a periodicity of 2.74 Å by a stick-slip motion along the Y direction. This predicted behavior and periodicity agree well with the observed sawtooth behavior and experimentally estimated periodicity of 2.7 ± 0.3 Å in Fig. 3(a). Across the scan direction, the tip apex will move an alternate constant distance of 1.58 Å due to the slip motion, which will induce the square-wave behavior of a constant amplitude 1.58 Å with the periodicity of 5.48 Å on f_X. The sharp steplike rise and fall in the square-wave behavior of f_X will synchronize with the sharp raise in the sawtooth behavior of f_Y. This predicted behavior and periodicity well agree with the observed square-wave behavior and the experimentally estimated periodicity of 5.4 ± 0.6 Å in Fig. 3(a). The predicted synchronism also agrees with the observed synchronism shown in Fig. 3(a).

On the other hand, for the fast-line scan toward the X direction, the tip apex will a take straight walk with the stick-slip motion, as shown in Fig. 3(c). Thus f_X will show the well-known sawtooth behavior with a periodicity of 3.16 Å by the stick-slip motion. This predicted behavior and periodicity agree well with the observed sawtooth behavior and experimentally estimated periodicity of 3.1 ± 0.3 Å in Fig. 3(b). Across the scan direction, the tip apex will not move, which will induce no fine structure in f_Y. This predicted behavior of no fine structure also agrees well with the observed signal in Fig. 3(b). Moreover, the amplitude of the sawtooth behavior in f_X is $C\Delta x$, where $\Delta x = f_X/k_X$ should agree with the periodicity of 3.16 Å. Using this assumption, we calibrated the value of C, and then determined the amplitude of the square-wave behavior in f_X shown in Fig. 3(a) as 1.6 ± 0.2 Å, which agrees well with the expected zigzag walk width of 1.58 Å. Thus the two-dimensional stick-slip model shown in Fig. 3(c) can explain the data of f_X in Figs. 3(a) and 3(b) fully; i.e., not only the periodicity but also the wave form and amplitude of the signals.

The motion of the tip apex described by the two-dimensional stick-slip model could be interpreted as two-dimensionally discrete jumps between spatially discrete adhesive points (stick points) with the same periodicity as

the lattice structure of the MoS_2 surface. Thus the friction which induces the tip apex motion also could be interpreted as a spatially discrete friction with the lattice periodicity. Theoretical studies and molecular-dynamics simulations on atomic-scale friction predicts the two-dimensional motion of the single atom, which is similar to the tip motion apex described by the two-dimensional stick-slip model.[19–22] These studies are based on the fact that the motion of a single atom is the interplay of the compliance of the friction system and the interaction between the single atom and an atomically flat surface.[2]

C. Fluctuation of the spatially discrete friction

Due to the slow scan, the way the tip apex moves due to the stick points, such as the zigzag walk or the straight walk shown in Fig. 3(c), will change. Therefore, we investigated the change of the fast-line-scan data, i.e., the change of the direction of the stick points such as the zigzag walk or straight walk. We assume that due to the slow-scan, the scan line position is changed step by step toward the direction orthogonal to the fast-line-scan direction with a 0.1-Å interval per fast-line scan. Here the scan line refers to the way the tip apex traces with the fast-line scan if there are zero deflection and torsion.

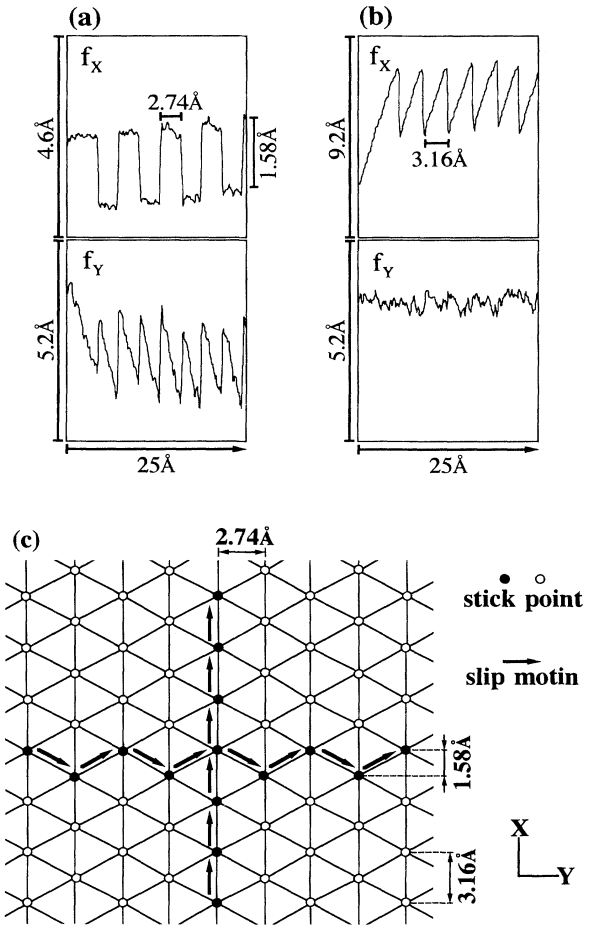

FIG. 3. (a) Typical data for f_X and f_Y (two-dimensional frictional-force vector components) due to a single fast-line scan along the cantilever (along the Y direction). The values f_X and f_Y are experimentally estimated values assuming the amplitudes of the sawtooth behaviors are equal to their periodicities. (b) Typical data due to a single fast line-scan across the cantilever (along the X direction). (c) The two-dimensional stick-slip model. The closed circle arrangements for the Y and X directions represent the trace of the tip apex, which explains the data shown in (a) and (b), respectively.

1. Fast-line scan across a row of stick points (along the Y direction)

Figures 4(a)–4(c) show fast-line-scan data for the fast-line scan across a row of stick points (along the Y direction), where the scan line position of each datum was changed due to the slow scan. Figures 4(a) and 4(c) correspond to parts of the image at the lower and upper thin arrows in Fig. 2(a), respectively.[23] Figure 4(b) corresponds to a part of the image between these two thin arrows in Fig. 2(a). In Fig. 4(a), f_X and f_Y show synchronized square-wave and sawtooth behaviors similar to Fig. 3(a). This behavior is understood by the tip apex motion of the regular zigzag walk, between the stick points on the α and β lines, as illustrated in Fig. 5(a).

In Fig. 4(b), f_X and f_Y also show synchronized square-wave and sawtooth behaviors, although three of the square waves are inverted. This behavior is understood by the fluctuated zigzag walk, where the tip apex walks on the stick points not only on α and β lines but also on the γ line, as illustrated in Fig. 5(b). Here we define the top, middle, and bottom levels of the square-wave behavior in f_X shown in Fig. 4, corresponding to stick points on the lines of α, β, and γ, respectively, shown in Fig. 5. In Fig. 4(c), f_X and f_Y show synchron-

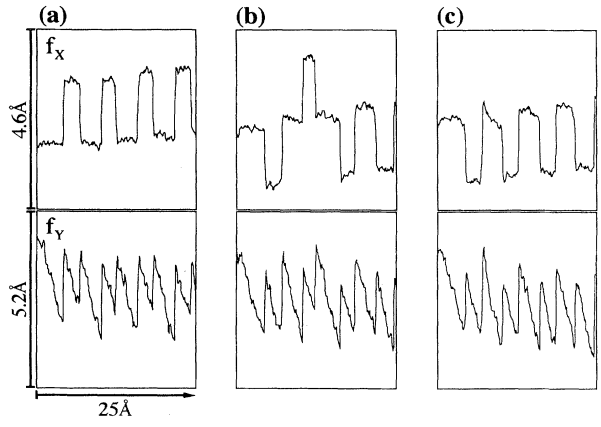

FIG. 4. (a)–(c) show fast-line-scan data for a fast-line scan across a row of stick points, where the scan line position of each data point changes toward the X direction due to the slow scan. These data are parts of images between the two thin arrows in Fig. 2(a).

ized square-wave and sawtooth behaviors, where all the square waves are inverted. This behavior is understood with the tip apex motion of the regular zigzag walk between the stick points on β and γ lines, as illustrated in Fig. 5(c). Thus, due to the slow scan, the regular zigzag walk between α and β lines shown in Fig. 5(a) is shifted to β and γ lines shown in Fig. 5(c) toward the slow-scan ($=X$) direction. During this shift, the zigzag walk shows the fluctuation illustrated in Figs. 5(b).

These changes of the tip apex motion along the slow-scan direction suggest that, due to the slow scan, the regular way the tip apex moves along the stick points changes, not suddenly, but fluctuating between two regular ways. Thus, along the slow scan direction, there seem to exist two states which follow one another repeatedly. One shows the regular zigzag walk of the tip apex, which could be interpreted as a stable state. The other, in which the tip apex moves between two adjacent regular zigzag ways, showing fluctuation, could be interpreted as an unstable state.

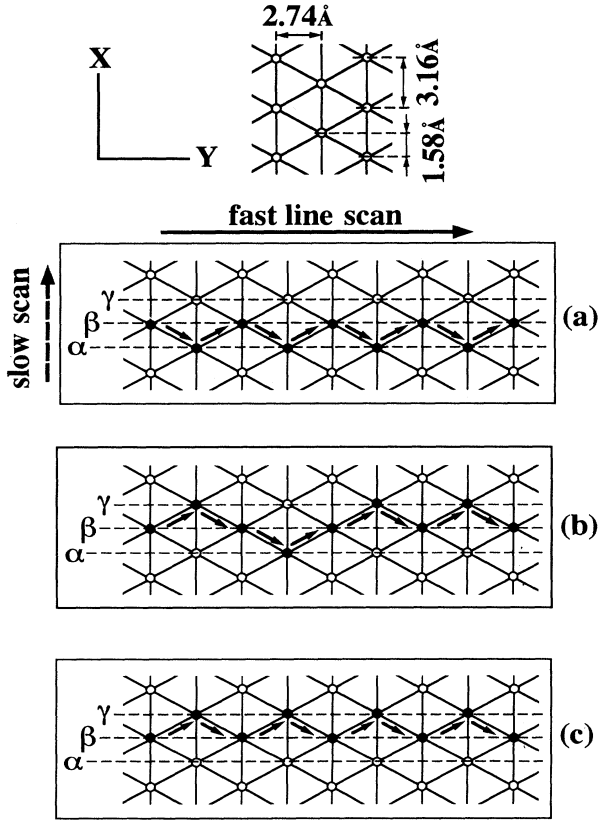

FIG. 5. (a)–(c) show the tip apex motions which explain the fast-line-scan data shown in Figs. 4(a)–4(c), respectively, based on the two-dimensional stick-slip model. The stick points on α, β, and γ lines correspond to top, middle, and bottom flat levels of the square wave in f_X shown in Fig. 4.

2. *Fast-line scan along a row of stick points (along the X direction)*

Figures 6(a)–6(c) show fast-line-scan data for the fast-line scan along a row of stick points (along the X direction), where the scan line position of each datum was changed due to the slow scan. Figures 6(a) and 6(c) correspond to parts of the image at the lower and upper thin arrows in Fig. 2(b), respectively.[23] Figure 6(b) is a part of the image between these two thin arrows in Fig. 2(b). In Fig. 6(a), f_X shows sawtooth behavior while f_Y shows no fine structure, similar to Fig. 3(b). This behavior is understood by the tip apex motion of the straight walk, where the tip apex moves on only one row of the stick points on the ζ line, as illustrated in Fig. 7(a).

In Fig. 6(b), f_X shows a sawtooth behavior consisting of 11 small slip signals, while f_Y shows six square-wave behaviors with a constant amplitude synchronized with the small slip signals in f_X. This behavior is explained by the fluctuation of the tip apex shown in Fig. 7(b), where the tip apex performs an almost regular zigzag walk between ζ and η lines. The periodicity of the small sawtooth behavior in Fig. 6(b) is 1.6 ± 0.2 Å, which agrees well with the expected width of the zigzag walk of 1.58 Å in the model of Fig. 7(b).

The amplitude of the sawtooth behavior of f_Y shown in Fig. 3(a) is $B\Delta y$, where $\Delta y = f_Y/k_Y$ should agree with a periodicity of 2.74 Å. Using this assumption, we calibrated the value of B, and then determined the amplitude of the square-wave behavior in f_Y shown in Figs. 6(b) to be 2.8 ± 0.3 Å, which agrees well with the expected zigzag walk width of 2.74 Å. Thus we confirmed that the two-dimensional stick-slip model is the first one that can fully explain both data of f_X and f_Y due to the two-dimensionally discrete friction, i.e., not only the periodi-

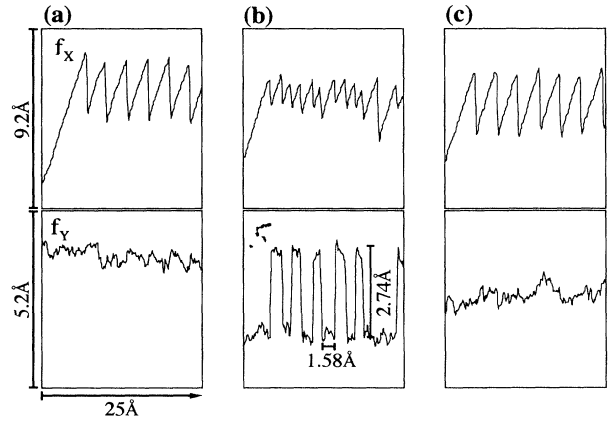

FIG. 6. (a)–(c) show fast-line-scan data for a fast-line scan along the row of stick points, where the scan line position of each data point changes toward the Y direction due to the slow scan. These data are parts of images between the two thin arrows in Fig. 2(b).

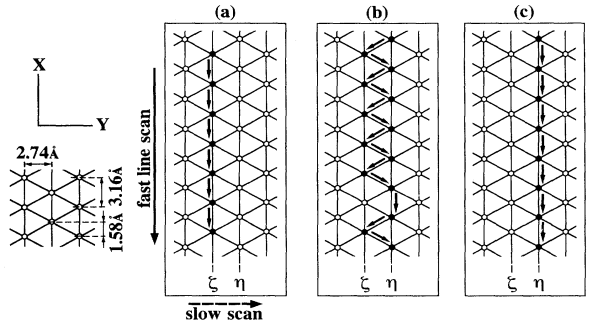

FIG. 7. (a)–(c) explain fast-line-scan data shown in Figs. 6(a)–6(c), respectively, based on the two-dimensional stick-slip model. The stick-point rows on ζ and η lines represent upper and lower flat levels of the square wave in f_Y shown in Fig. 6.

city but also the wave form and amplitude of the signal. Table I shows a comparison between theoretical values based on the two-dimensional stick-slip model and experimentally estimated values of periodicities and amplitudes of f_X and f_Y. We mention that the two-dimensional stick-slip model is the first one that can explain not only periodicity (horizontal axis) but also amplitude (vertical axis), as well as the wave form of the data of the atomic scale.

In Fig. 6(c), f_X shows a sawtooth behavior with only large slip signals, while f_Y shows no fine structure, similar to Fig. 6(a). Compared with Fig. 6(a), however, the phase of the sawtooth signal changed by π, and the dc level of f_Y changed from upper to lower levels of the square-wave behaviors. This phase change of the sawtooth signal is understood by the 1.58-Å position shift of the stick points along the X direction between ζ and η lines, as shown in Fig. 7. The dc level change in f_Y is understood by the distance of 2.74 Å between ζ and η lines along the Y direction as shown in Fig. 7.

Thus, due to the slow scan, the straight walk shifted from the ζ line in Fig. 7(a) to the η line in Fig. 7(c) toward the slow scan ($=Y$) direction. During this shift, the straight walk shows the fluctuation illustrated in Fig. 7(b).

These changes of the tip apex motion along the slow scan direction suggest that, due to slow scan, the way the tip apex moves along the stick points changes, not suddenly, but fluctuating between two straight ways. Thus, along the slow scan direction, there seem to exist two states which follow one another repeatedly.[9] In one, the tip apex performs a straight walk, which could be interpreted as a stable state. In the other, the tip apex moves between two adjacent straight ways, showing fluctuation, which could be interpreted as an unstable state.

D. Two-dimensional stick-slip model with effective adhesive radius

As described above, based on the two-dimensional stick-slip model, (1) wave forms of sawtooth and square-wave behaviors, (2) averaged periodicities of sawtooth and square-wave behaviors, and (3) amplitudes of square-wave behavior, are explained. However, questions like (4) what changes sticking to slippage (or where does the slip occur), (5) what causes the small unevenness of the peak value in the sawtooth behavior and the asymmetry of the interval in the sawtooth and square-wave behaviors [due to each discrete jump, as shown in Figs. 3(a) and 4], and (6) which is the nearest stick point (or which stick point will be the nearest one to which the tip apex can jump) cannot be explained by the simple two-dimensional stick-slip model. Here, in order to explain these questions, we expand the two-dimensional stick-slip model by introducing an effective adhesive radius.

1. Effective adhesive radius

For simplicity, we assume that spring constants along and across the cantilever (Y and X directions) are the same, and that the sticking force (adhesive force, i.e., f_{adh}) is constant and independent of direction. In order to explain question (4), we assume that the effective adhesive radius determines the place where the tip apex

TABLE I. Theoretical and experimental values of square-wave and sawtooth behaviors on MoS_2 based on the two-dimensional stick-slip model.

			Theoretical	Experimental
(scan along Y)	f_X	periodicity	5.48 Å	5.4±0.6 Å
scan across a row	square wave	amplitude	1.58 Å	1.6±0.2 Å
of stick-points	f_Y	periodicity	2.74 Å	2.7±0.3 Å
	sawtooth	amplitude	2.74 Å	$\Delta y \equiv 2.74$ Å
(scan along X)	f_X	periodicity	3.16 Å	3.1±0.3 Å
scan along a row	sawtooth	amplitude	3.16 Å	$\Delta x \equiv 3.16$ Å
of stick-points	f_Y	periodicity	3.16 Å	3.1±0.3 Å
	square wave	amplitude	2.74 Å	2.8±0.3 Å

slips, as follows. Hereafter, we use the notations $\perp$ and $\parallel$, which refer to across and along the fast-line-scan direction, respectively.

As shown in Fig. 8(a), the distance a between the stick point and the scan line creates the force component of $f_\perp = k_\perp a$ across the scan direction. Here, the scan line means the way in which the tip apex traces with the fast-line scan if there are zero deflection and torsion, and the stick point corresponds to the point where the both force components are zero. This $f_\perp$ works against the sticking force in addition to the ordinary force component of $f_\parallel$ along the scan direction. When $f_\parallel = k_\parallel b$, the resultant force of these force components $(f_\perp^2 + f_\parallel^2)^{1/2}$ becomes equal to the sticking force of f_{adh}, and the tip apex slips, which is expressed as

$$f_{\text{adh}}^2 = f_\perp^2 + f_\parallel^2 = (k_\perp a)^2 + (k_\parallel b)^2 . \tag{8}$$

Hereafter, we call this the slip place. We simplify to

$$k_\perp = k_\parallel \equiv k , \tag{9}$$

so that

$$f_{\text{adh}}^2 = k^2(a^2 + b^2) . \tag{10}$$

Since

$$f_{\text{adh}}^2 / k^2 \equiv r^2 \tag{11}$$

is a constant value independent of a and b, we have

$$a^2 + b^2 = r^2 . \tag{12}$$

This means that this stick place traces an arc with a radius of r, by the change of the distance a due to the slow scan, as shown in Fig. 8(a). Therefore, we call r the effective adhesive radius. Here the slip place is also regarded as the cross-point of effective adhesive radius and the scan line.

Thus $f_\perp$ is determined by the distance a, which is constant during the sticking and determines the value from the zero force, i.e., the absolute value of the flat area in the square-wave behavior as shown in Fig. 8(b). On the other hand, $f_\parallel$ changes linearly by the fast-line scan during the sticking, and reaches a peak value just before the slip, which is determined by the distance b as shown in Fig. 8(b). The distance b also determines the interval of the sticking, where b is determined by r and a through Eq. (12).

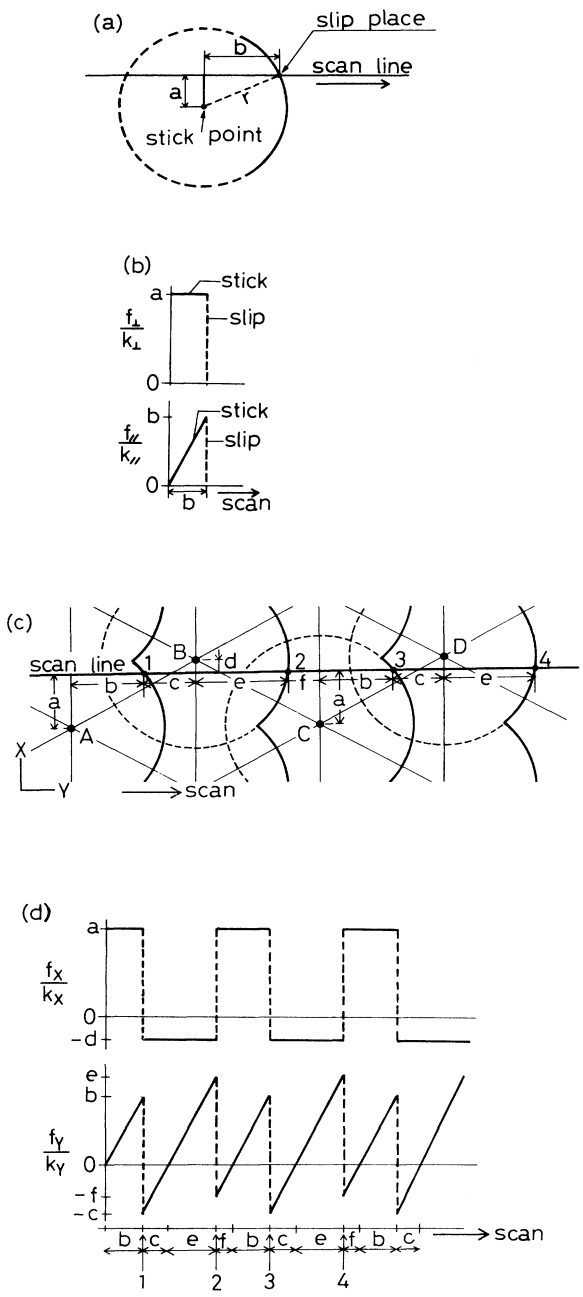

FIG. 8. (a) Effective adhesive radius corresponds to the trace of the slip place, where sticking changes to slipping, with a change of scan line position due to the slow scan. Thus the slip place is determined by the cross point of the scan line and the effective adhesive radius. (b) Predicted behavior of $f_\perp$ and $f_\parallel$ due to the single effective adhesive radius shown in (a). (c) Extended two-dimensional stick-slip model with an effective adhesive radius, where the fast-line-scan direction is across the row of the stick points, i.e., $X = \perp$ and $Y = \parallel$. (d) Predicted behavior of $f_X (f_\perp)$ and $f_Y (f_\parallel)$ based on the model shown in (c).

2. *Two-dimensional stick-slip model combined with effective adhesive radius*

In order to explain questions (5) and (6), we combine the effective adhesive radius and two-dimensional stick-slip model as shown in Fig. 8(c), where the fast-line-scan direction is across a row of the stick points, i.e., $X = \perp$ and $Y = \parallel$. Just before the slip from the stick point A at the slip place 1, similarly to Fig. 8(a), the effective adhesive radius r and the distance a determine the absolute values of both f_X and f_Y and the interval of the sticking, as shown in Fig. 8(d) similarly to Fig. 8(b). Then, since the slip place 1 is located in the effective

adhesive radius of stick point B, the tip apex will jump to the stick point B as the nearest stick point.

Just after stick to stick point B, absolute values of f_X are determined by the distance d. On the other hand, absolute values of f_Y are determined by the distance c, which is a minimum value as shown in f_Y/k_Y of Fig. 8(d). Thus the absolute values of both f_X and f_Y just after the slip are determined by the vector, i.e., both distances along X and Y between the slip place and the next stick point.

During stick to stick point B, the absolute value of f_X takes a constant value determined by the distance d, which forms the flat lower area in the square-wave behavior between 1 and 2 shown by f_X/k_X in Fig. 8(d). On the other hand, the absolute value of f_Y changes linearly by the fast-line scan, and reaches another peak value which is determined by the distance e just before the slip at slip place 2. Here distances d and e are assumed to satisfy the relation

$$d^2+e^2=r^2 , \tag{13}$$

similarly to Eq. (12). Further since slip place 2 is located in the effective adhesive radius of stick point C, the tip apex will jump to the stick point C.

When the tip apex slips from stick points B to C at slip place 2, absolute values of f_X/k_X and f_Y/k_Y change from $-d$ to a and from e to $-f$, respectively, as shown in Fig. 8(d). Here

$$b+c=e+f=2.74 \text{ Å} \tag{14}$$

(orthography of the lattice constant to the scan direction: 3.16 Å $\times \sin 30°$) and

$$a+d=1.58 \text{ Å} \tag{15}$$

can be obtained as shown in Fig. 3(c).

During stick to stick point C, the absolute value of f_X takes a constant value determined by the distance a, which forms the flat upper area in the square-wave behavior between 2 and 3 shown by f_X/k_X in Fig. 8(d). On the other hand, the absolute value of f_Y changes linearly by the fast-line scan, and reaches a peak value just before the slip which is determined by the distance b. Thus the stick points A and C produce exactly the same behaviors as f_X and f_Y, and the behaviors between 1 and 3 shown in Fig. 8(d) are repeated by the fast-line scan.

Based on this model, f_Y ($f_\parallel$) shows sawtooth behavior with alternating high and low peak values just before and after the slip, which are determined by the distances b, c, e, and f. These two types of sawtooth behaviors with high and low peak values have slightly different intervals of $c+e$ and $b+f$, while those two intervals together have a constant periodicity of

$$c+e+f+b=5.48 \text{ Å} \tag{16}$$

from Eq. (14). On the other hand, f_X ($f_\perp$) shows square-wave behavior synchronized with sawtooth behavior, where the upper and lower absolute values of the flat areas are determined by the distances a and d although the resultant amplitude is a constant value of 1.58 Å from Eq. (15). These explain the small unevenness of the peak value in the sawtooth behavior, and the asymmetry of the intervals of sawtooth and square-wave behaviors due to each discrete jump, as shown in Figs. 3(a) and 4. We mention that, by using this model, we can deduce the absolute values of the both force components, or fast line-scan data toward the arbitrary direction, quantitatively.

Further, we mention that the effective adhesive radius introduces the effect of the compliance of the cantilever into the two-dimensional stick-slip model, which is indicated by Eq. (10). Thus this extended model suggests that phenomenon described above is an interplay of the compliance of the cantilever and the interaction between the tip apex and the atomically flat surface, which is consistent with the theoretical analysis.[2,19–22]

V. CONCLUSION

The two-dimensional stick-slip phenomenon implies that, on an atomic scale, the frictional force acts not only along the scan direction but also across the scan direction, which is contradictory to the assumption of the friction on a macroscopic scale. This means that the fundamental assumption of classical friction on a macroscopic scale shows a breakdown on the atomic scale.

The motion of the tip apex described by the two-dimensional stick-slip model could be interpreted as two-dimensionally discrete jumps between spatially discrete adhesive points with the same periodicity as the lattice structure of the MoS_2 surface. Thus the friction which induces the motion of the tip apex also could be interpreted as a spatially discrete friction with the lattice periodicity. This spatially discrete friction shows the fluctuation. Further, the nature of the spatially discrete friction was explained in more detail by the two-dimensional stick-slip model with an effective adhesive radius, which introduced the effect of the compliance into the two-dimensional stick-slip model.

ACKNOWLEDGMENTS

We thank Dr. T. Okada, S. Mishima, and S. Ito of Olympus Optical Co., Ltd. for the construction of the AFM/LFM unit. We also thank A. Toda and K. Matuyama of Olympus Optical Co., Ltd. for supplying the Si_3N_4 microcantilevers.

[1]F. P. Bowden and D. Tabor, *The Friction and Lubrication of Solids* (Clarendon, Oxford, 1954).

[2]C. M. Mate, G. M. McClelland, R. Erlandsson, and S. Chiang, Phys. Rev. Lett. **59**, 1942 (1987).

[3]R. Erlandsson, G. Hadziioannou, C. M. Mate, G. M. McClelland, and S. Chiang, J. Chem. Phys. **89**, 5190 (1988).

[4]G. J. Germann, S. R. Cohen, G. Neubauer, G. M. McClelland, and H. Seki, J. Appl. Phys. **73**, 163 (1993).

[5]R. Kaneko, K. Nonaka, and K. Yashuda, J. Vac. Sci. Technol. A **6**, 291 (1988).

[6]C. M. Mate, Phys. Rev. Lett. **68**, 3323 (1992).
[7]E. Meyer, R. Overney, D. Brodbeck, L. Howald, R. Lüthi, J. Frommer, and H.-J. Güntherodt, Phys. Rev. Lett. **69**, 1777 (1992).
[8]S. Fujisawa, Y. Sugawara, S. Ito, S. Mishima, T. Okada, and S. Morita, Nanotechnology **4**, 138 (1993).
[9]S. Fujisawa, E. Kishi, Y. Sugawara, and S. Morita, Jpn. J. Appl. Phys. **33**, 3752 (1994).
[10]S. Fujisawa, Y. Sugawara, and S. Morita, Microbeam Anal. **2**, 311 (1993).
[11]S. Fujisawa, M. Ohta, T. Konishi, Y. Sugawara, and S. Morita, Rev. Sci. Instrum. **65**, 644 (1994).
[12]G. Meyer and N. M. Amer, Appl. Phys. Lett. **57**, 2089 (1990).
[13]O. Marti, J. Colchero, and J. Mlynek, Nanotechnology **1**, 141 (1990).
[14]Y. Sugawara, T. Ishizaka, S. Morita, S. Imai, and N. Mikosiba, Jpn. J. Appl. Phys. **29**, L502 (1990).
[15]S. Akamine, R. C. Barrett, and C. F. Quate, Appl. Phys. Lett. **157**, 316 (1990).
[16]H. Heinzelmann, E. Meyer, D. Brodbeck, G. Overney, and H.-J. Güntherodt, Z. Phys. B **88**, 321 (1992).
[17]J. A. Wilson and A. D. Yoffe, Adv. Phys. **18**, 193 (1969).
[18]Olympus Optical Co., Ltd., 2951 Ishikawacho Hathioji, 192 Japan.
[19]M. Hirano and K. Shinjo, Phys. Rev. B **47**, 11 837 (1990).
[20]J. A. Harrison, C. T. White, R. J. Colton, and W. B. Brenner, Phys. Rev. B **46**, 9700 (1992).
[21]K. Shinjo and M. Hirano, Surf. Sci. **283**, 473 (1990).
[22]J. A. Harrison, C. T. White, R. J. Colton, and W. B. Brenner, J. Phys. Chem. **97**, 6573 (1993).
[23]See AIP document no. PAPS PRBMDO-51-7849-5 for 5 pages of "all fast line-scan data between two thin arrows in Figs. 2(a) and 2(b)." Order by PAPS number and journal reference from American Institute of Physics, Auxiliary Publication Service, Carolyn Gehlbach, 500 Sunnyside Boulevard, Woodbury, New York, 11797. Fax: 516-576-2223, e-mail: janis@aip.org. The price is $1.50 for each microfiche (98 pages) or $5.00 for photocopies of up to 30 pages, and $0.15 for each additional pages over 30 pages. Airmail additional. Make checks payable to the American Institute of Physics.

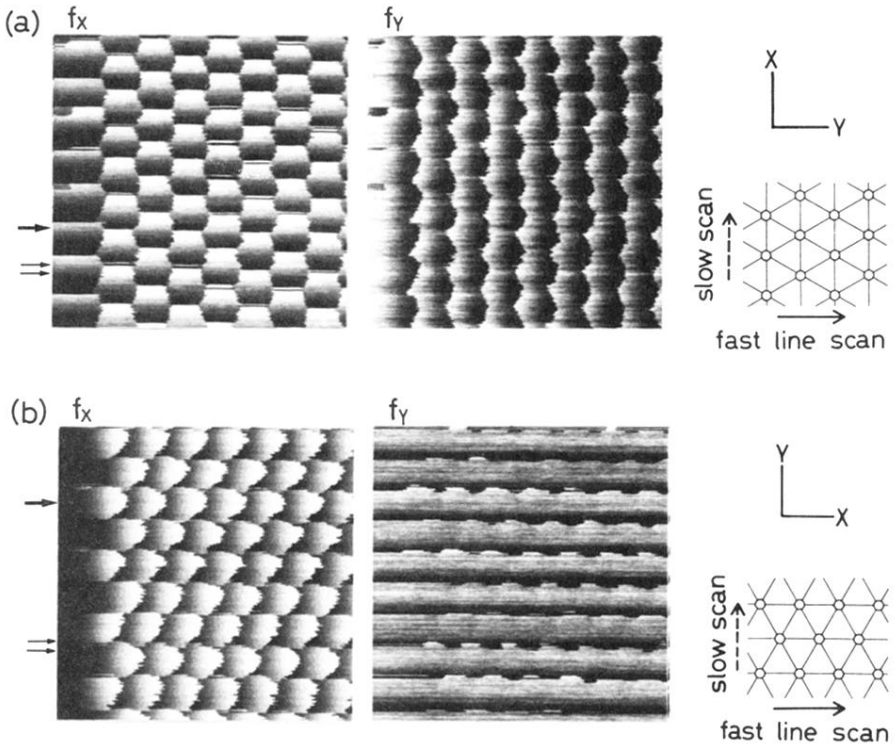

FIG. 2. f_X and f_Y images for the fast-line-scan directions (a) along the cantilever (along the Y direction) and (b) across the cantilever (along the X direction). Scan area is 25×25 Å^2. Beside each image, schematic views of the lattice structure of the observed MoS_2 surface are shown.